Analog Integrated Circuits and Signal Processing, 29, 127–149, 2001

Mixed-Technology System-Level Simulation

J. A. MARTINEZ,[1] T. P. KURZWEG,[1] S. P. LEVITAN,[1]* P. J. MARCHAND[2] AND D. M. CHIARULLI[1]

[1] *University of Pittsburgh, Pittsburgh, PA 15261, USA*
[2] *Optical Micro Machines, San Diego, CA 92121, USA*

Abstract. This paper describes a computationally efficient method to simulate mixed-domain systems under the requirements of a system-level framework. The approach is the combined use of Modified Nodal Analysis (MNA) for the representation of a mixed-technology device and piecewise linear (PWL) techniques to overcome the costly numerical evaluation found in conventional circuit or device simulators. This approach makes the simulation computationally fast, as well as more stable when compared with traditional circuit simulation. The PWL solver, based in the frequency domain, is more robust to inconsistencies in initial conditions and impulse changes when compared to integration based solvers in the time domain. The advantage of this method is that the same solver enables the integration of multi-domain devices (e.g., electrical, optical, and mechanical) in the same simulation framework. The use of this technique for the simulation of multi-domain systems has proven to give better performance in simulation time when compared to traditional circuit simulators with a relatively small decrease in the level of accuracy. Comparisons with traditional solvers, such as SPICE, show two to three orders of magnitude speedup with less than 5% relative error. The ability to adjust the level of accuracy, either by varying the sampling rate or the number of regions of operation in the models, allows for both computationally fast and in-depth analysis in the same CAD framework.

Key Words: MEM simulation, modified nodal analysis (MNA), optical MEM CAD tool, piecewise linear simulation (PWL), optoelectronic simulation, microsystem modeling and simulation

1. Introduction

Applications for optical MEMS (micro-electrical-mechanical systems), or MOEMS, are growing to include switching, scanning, projection, display, printing, sensing, modulating, and data storage [1]. As these applications transition from abstract ideas to marketable products, the cost of designing, prototyping, and testing these systems has slowed down this development time. Instead of physically prototyping these systems, computer aided design (CAD) tools can greatly reduce the cost and time of marketing an optical MEM product. This has been seen in the past 30 years in the VLSI revolution. Using CAD tools, integrated circuits were designed, fabricated, and the time-to-market was decreased significantly, while the likelihood of a successful first physical prototype increased. However, like many new technologies, design methods and tools for optical MEM systems are currently ad-hoc. Designers typically use combinations of tools that were built for the individual domains of optics, mechanics, and electronics with little integration and with system-level analysis based only on the experience of the designer or simply on assumptions about the ensemble behavior of the components.

In order to support the design of mixed-signal optical MEM systems, computer aided design tools must be capable of modeling, electronics, electrostatics, mechanics, guided wave optics, and free space optics. The design tools must directly support the interactions between models in all these domains, and characterize the behavior of the resulting system in an interactive environment. Obviously, CAD tools exist in each of these specialized domains and it is unnecessary to reinvent these tools. For example, SPICE is the standard

* Address correspondence to: E-mail: steve@ee.pitt.edu; www:http://kona.ee.pitt.edu/pittcad; Tel.: 412 648 9663; Fax: 412 624 8003.

simulation technique for electrical circuits and devices. Code V [2] and ASAP [3] are available for accurate optical modeling, and CAD tools for conventional MEMS are being designed in both academia and industry, including those by CMU [4], Conventor [5], and MEMScaP [6]. However, these tools do not provide a single multi-domain design environment, which is needed for modeling mixed-technology applications.

This paper concentrates on the system-level modeling and simulation of optical MEM systems, focusing particularly on the electrical and mechanical signals and component models appropriate for a mixed-signal, interactive CAD tool. The rest of this paper is organized as follows. In the next section, we present an overview of previous work related to the present research and an introduction to our optical MEM system-level simulator, Chatoyant. This is followed by a description of the piecewise linear technique for the simulation of nonlinear networks in Section 3, with an application of this technique for the simulation of optoelectronic devices being developed in Section 4. Section 5 introduces the application of our piecewise linear technique for the simulation of micro-mechanical devices. In Section 6, a series of example systems are presented to illustrate our techniques and, finally, we close with a summary and conclusions.

2. Background

2.1. Mixed Signal, Multi Domain Simulation

The need to support modeling of various technology domains in an optical MEM design leads us to evaluate the impact of having heterogeneous signals in a common simulation framework. An optical MEM design environment needs to support electronic, mechanical, and optical components, with the possibility of extensions to other domains, such as thermal, chemical, and RF. Not only do we have to characterize the sets of interactions between components of different technologies, we also have to consider the performance of the simulation environment, which depends on the simulation method and the type of signal characterization chosen.

Several research efforts have been conducted to offer a suitable methodology for the simulation of these systems. They can be classified into two different approaches: behavioral modeling and equivalent circuit methods.

Behavioral modeling is a flexible and general methodology that allows hierarchical support and mixed signal simulation. Hardware description languages with extensions to support analog signals such as VHDL-AMS or Verilog-A are used to describe the system. In this approach, the degree of abstraction obtained with the hardware description language simplifies the designer's task for the description of the system. A mixed signal CAD tool is used as the simulation framework. Consequently, the support for co-simulation is already in place. This methodology is applied in the simulation of optical MEM systems in [7,8].

Even though the behavioral modeling approach appears to be a promising option for the modeling of mixed-signal, multi-domain systems, it is necessary to clarify the difficulties and limitations present in this technique. During the description of the system, the designer must specify the relations that define the interaction between the different signals in the system. The definition of these relationships is a very active area of research. It involves the characterization of ports, defined as transducers (energy conversion devices), and elements, defined as actuators (unidirectional energy flow devices), as explained in [9]. Additionally, this technique relies on the abstraction levels offered by the mixed-simulation framework and, in doing so, it shares its drawbacks as well. For example, mixed-signal, multi-domain micro-systems consisting of a large number of elements result in large computation loads.

The second approach for modeling mixed-signal multi-domain systems is based on finding an electrical equivalent representation for the non-electrical domain required to be simulated. The electrical equivalent can be simulated using any of the well known and established circuit simulators (e.g., SPICE, SABER, iSMILE [10,11]). This method has been used in [12–14] for the simulation of micro mechanical devices, where a mapping of these devices to a SPICE netlist is proposed. In [10] Yang simulates optoelectronic interconnection links using iSMILE as the circuit simulator engine. The limitations of this technique are the lack of support for hierarchical design and co-simulation. Because the simulation is coupled to an analog simulator, digital simulation is not supported.

The advantage of traditional circuit simulators, based on numerical integration solvers, is that they provide good accuracy when solving the linear and nonlinear differential equation (DE) systems. The problems associated with these circuit simulators are their

reliability and long computation times. It is also well known that there are non-convergence problems faced during simulation of electronic circuits [15]. These techniques become computationally expensive with increasing size of the network being analyzed and when the network has a high degree of non-linearity. The use of such a computationally intense algorithm as the core for an interactive CAD tool would make this application inefficient.

As an alternative to traditional circuit simulation, a non-linear network modeling technique using piecewise linear (PWL) models was added to the timing simulator IRSIM by Kao [16] and Horowitz [17]. This technique is well suited for the delay estimation in dense non-linear digital-VLSI networks. However, the limited complexity of the MOSFET models and tree analysis technique used in this method do not allow piecewise linear timing analyzers to simulate higher order effects, which are of significant importance in the modeling of mixed signal devices or analog simulation in general.

Even with the limitations of the previous work, piecewise modeling has been an intense area of research as a potential alternative to numerical integration in the simulation of analog dynamic systems. The principle behind this approach is the segmentation of a complex analytical expression into regions of operation that can be characterized by simplified mathematical sub-functions. These sub-functions are chosen to closely match the original function but are computationally more tractable.

This technique has been applied with relative success in simulators such as NECTAR 2 [18], PLANET [19], and PLATO [20]. These simulators are much more stable when compared to traditional circuit simulators and provide flexibility for their use in hierarchical design.

In these simulators, the complete PWL representation of the system is introduced using ideal switches (diodes) to reconfigure regions. Mathematically, there is a set of step, or activation, functions that allow for the complete translation of the non-linear representation to a linear complementary problem. The solution to the mathematical representation consists of a space divided into regions, where every one of these subspaces contains a linear solution to the system. The solution of the PWL problem consists of a search of this space for the regions where the system is satisfied at every timestep of the simulation run. Consequently, the iterative process (e.g., Newton-Raphson) found in conventional circuit simulators is entirely eliminated and translated into a search problem. The development of an efficient search algorithm that finds the solutions to the PWL problem has been the focus of numerous research efforts such as those found in [21–23].

However, conventional PWL simulators still use integration techniques to solve the transient response of the system because they consider continuous analog behavior for input signals. This is a more accurate approach, but computationally demanding because it requires integration techniques to solve the set of linear differential equations.

In this paper, we propose a PWL technique as the basis for analog simulation in a system-level framework. In our approach, we extend the piecewise technique to also represent the signals in the system. The input signals are linearized and, consequently, the transfer function for the system can be obtained explicitly. This decreases the computational requirements because it avoids the integration process required in the conventional algorithms.

Additionally, a direct representation for the system is used as the PWL mathematical representation. This avoids the computational overhead of using a superset, or union, of PWL models for the representation in the linear numerical analysis solver, which is the case for other PWL simulator implementations. The different configurations of the system are changed according to the change of regions of operation over individual non-linear components and not through the use of ideal switches that configure the superset model. Boundary conditions of individual non-linear components are used to determine the switching behavior between configurations.

The fact that the node density is moderate for the networks generated for the modeling of opto electromechanical devices in a modular environment allows us to consider piecewise linear modeling merged with linear numerical analysis as a way to achieve the desired accuracy with low computation demands.

Before we present the details of our PWL simulation techniques, we first introduce our system-level CAD framework in which these models are implemented.

2.2. Mixed-Signal Micro-Optical-Electro-Mechanical Simulation Tool: Chatoyant

The modeling methods presented throughout this paper have been implemented in our mixed-technology

simulator *Chatoyant*. Chatoyant is a multi-level, multi-domain CAD tool that has been successfully used to design and simulate free space optoelectronic interconnect systems [24]. Static simulations analyze mechanical tolerancing, power loss, insertion loss, and crosstalk, while dynamic simulations are used to analyze data streams with techniques such as noise analysis and bit error rate (BER) calculation. Optical propagation models are based on two techniques: Gaussian and diffractive scalar. Gaussian models give fast and accurate results for macro-scale systems and systems that exhibit limited diffraction, while more computationally intensive scalar models are used when diffraction effects dominate the system.

A Chatoyant schematic of a 1×2 optical MEM optical cross-connect [25] is shown in Fig. 1. In Chatoyant, each icon represents a component model with sets of parameters defining the characteristics of the component. Each line represents a signal path (either optical, mechanical, or electrical) connecting the outputs of one component to the inputs of the next. This system shows an optical fiber emitting light into a free space medium. The light then travels through a collimating lens, is reflected off of a switching mirror, through a second collimating lens and into an outgoing fiber. The mirror is assembled on an anchored cantilever beam, which bends into and out of the optical path by electrostatic attraction between the beam and the substrate. Three electrostatic forces are placed on the beam/mirror icon: on the x and z positions and a torque around the z axis. Above the schematic, we show an optical intensity distribution as light strikes the outgoing fiber, while, on the right of the figure, we show a dynamic waveform and eye-diagram from a data signal. Details of this system are given toward the end of the paper.

The actual approach for our modeling of mixed signal, multi-domain systems is a discrete event driven simulation model, which operates over the global system. An object-oriented framework, Ptolemy [26] is used to provide this degree of abstraction for the simulation of such systems. We choose Ptolemy's "Dynamic Data Flow" (DDF) Ptolemy simulation method as our discrete event engine. Timing information is added to support multiple and run-time-rate variable streams of data flowing through the system. In this model of computation, the simulation scheduler creates a dynamic schedule based on the flow of data between the modules. This allows modeling of multi-dynamic systems where every component can alter the rate of consumed/produced data at any time during simulation. The scheduler also provides the system with buffering capability. This allows the system to keep track of all the signals arriving at one module when multiple input streams of data are involved.

To maximize our modeling flexibility, our signals are composite types, representing the attributes of force,

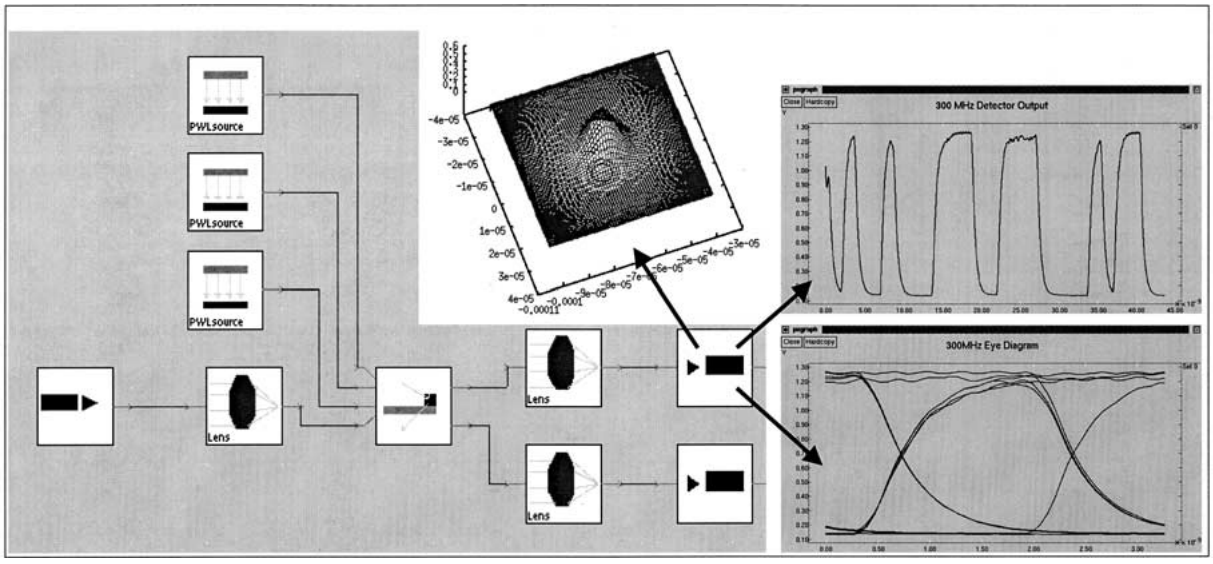

Fig. 1. Chatoyant analysis of an optical cross connect.

displacement, velocity, and acceleration for mechanical signals, voltages and impedances for electronic signals, and wavefront, phase, orientation, and intensity for optical signals. The composite type is extensible, allowing us to add new signal characteristics as needed.

Mixed-signal, multi-domain systems in Chatoyant have a conceptual and abstract representation consisting of a set of modules interchanging information. However, this simulation approach brings the challenge of developing the circuit/component modeling techniques that will be optimal for fast and accurate characterization of the different modules involved in this system. This challenge is the focus of the remainder of this paper.

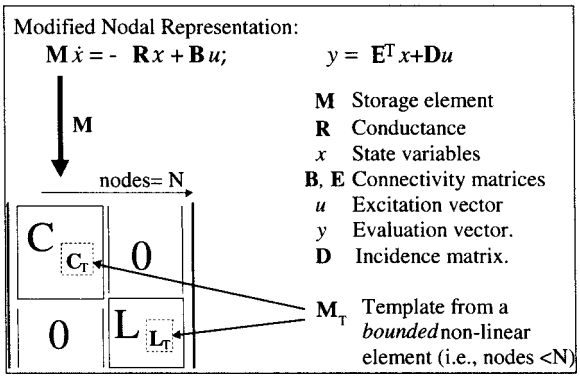

Fig. 3. MNA representation and template integration.

3. Methodology: Piecewise Linear Modeling

Considering each of our Chatoyant icons in Fig. 1 as device models consisting of a moderate number of nodes, we show how our device modeling is accomplished through the diagram in Fig. 2. We perform linear and non-linear sub-block decomposition of the circuit model of the device. This decomposes the design into a linear multi-port sub-block section and non-linear sub-blocks. The linear multi-port sub-block can be thought of as characterizing the interconnection network and parasitic elements while the non-linear sub-blocks characterize active non-linear behaviors.

In the second step, a Modified Nodal Analysis (MNA) [27] is used to create a mathematical representation for the devices, as shown in Fig. 3. Throughout this section we describe this representation in the electrical domain, without loss of generality, as we will show the same formulation applied to the mechanical domain in following sections. In this expression, **M** corresponds to the memory matrix of the system, also called the susceptance matrix, **R** is the conductance matrix, x is the vector of state variables, **B** is a connectivity matrix, u is the excitation vector, and the y vector contains the desired variables to evaluate.

The linear elements can be directly mapped to this representation, but the non-linear elements need to first undergo a further transformation. We perform piecewise modeling of the active devices for each non-linear sub-block. When we form each non-linear sub-block, a

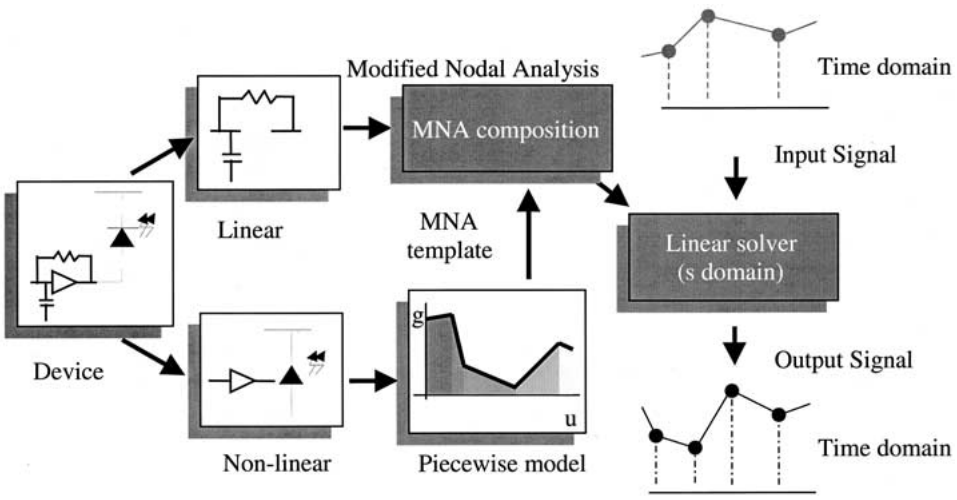

Fig. 2. Piecewise modeling for optoelectronic devices.

MNA template is used for each device in the network. The use of piecewise models is based on the ability to change these models for the active devices depending on the changes in conditions in the circuit, and thus the regions of operation.

The templates generated can be integrated to the general MNA containing the linear components adding their matrix contents to their corresponding counterparts. This process is shown in Fig. 3 for the storage, or memory, matrix **M**. This same composition is done for the other matrices. The size of each of the template matrices is bounded by the number of nodes connected to the non-linear element.

Once the integrated MNA is formed, a linear analysis in the frequency domain can be performed to obtain the solution of the system. Constraining the signals in the system to be piecewise linear in nature allows us to use a simple transformation from and to the time domain without the use of costly numerical integration. For a better understanding of our modeling technique, we next present some details of the modified nodal analysis representation.

3.1. Global Mathematical Representation of the Linear Time-invariant System: MNA

We have chosen MNA [28–30] as the technique to map the linear electrical network representation into a system of first-order differential equations and algebraic equations. For a development of this technique the reader can explore the work presented in [31,32]. This formulation, applied to the electrical domain as shown in Fig. 3, is based in the application of the KCL (Kirchoff's current law) over the nodal representation of the circuit and the use of the state variable definition $x = \binom{v}{i}$. In this state definition, $v \in \Re^n$ corresponds to the vector of voltage nodes in the network and $i \in \Re^m$ corresponds to a vector representing only the currents going through inductors, and sources in the network. What is accomplished with this state definition is a transformation from a second order ordinary differential equation (ODE) problem to a first order differential equation, at the expense of increasing the range of the linear problem from n to $(n + m)$.

The structure of the passive elements **R** and memory elements **M** is:

$$\mathbf{R} = \begin{bmatrix} \mathbf{G} & \mathbf{E} \\ -\mathbf{E}^{\mathbf{T}} & \mathbf{0} \end{bmatrix}; \quad \mathbf{M} = \begin{bmatrix} \mathbf{C} & \mathbf{0} \\ \mathbf{0} & \mathbf{L} \end{bmatrix}; \qquad (1)$$

$\mathbf{C} \in \Re^{n \times n}$ is the capacitance and $\mathbf{L} \in \Re^{m \times m}$ is the inductance matrices of the network. $\mathbf{G} \in \Re^{n \times n}$ represents the conductance $(1/R)$ elements of the network and $\mathbf{E} \in \Re^{m \times m}$ is the incidence matrix of i in every node. **B** and **D** represent node incidence matrices for the input sources of the system. **D** is an incidence matrix that allows one to obtain the desired set of variables y from the state variable vector x.

A useful feature of this representation is that the relative inclusion of any discrete element (e.g., R, C, L, and sources) can be expressed as a pattern or "template." As mentioned previously, each element type can be described as a set of specific **R**, **M**, and **B** matrices. This set, or template, can then be used to introduce the element into the global MNA, requiring only its position in terms of a nodal index. The following section describes the mapping of the different classes of elements to the MNA representation.

Mapping of Passive Elements to the MNA

A simple example will help to clarify how passive elements (R, C, L) are introduced into the global MNA. Consider the circuit in Fig. 4.

The MNA representation for the linear circuit shown in Fig. 4, according to the equations found in Fig. 3 is shown in Fig. 5.

The capacitors and resistors are added to the **M** and **R** matrices according to their nodal index at their terminals. As in the well known KCL method, when building this representation the rows of the matrix equation correspond to the nodes in the circuit. Also, the columns in each matrix have the same index order. As an example, node a corresponds to the first row in Fig. 5. The addition of all the capacitors connected to node a, C^1, is the value to put in location a,a of the matrix **M**. The rest of the elements on the row of **M** correspond to capacitors connected between a and the rest of the nodes. In this example, the only element not zero is a,b because C^1 is also connected to this node. The value of these elements must be negative because they corresponds to currents that are coming into the node a, which is opposite to the accepted positive direction. Elements that are connected to ground on one end, such as G^2 in the example, only have contribution to the non-ground node (c for G^2). This is because the reference node, ground, is not explicitly used, since it is used as a reference for all potentials.

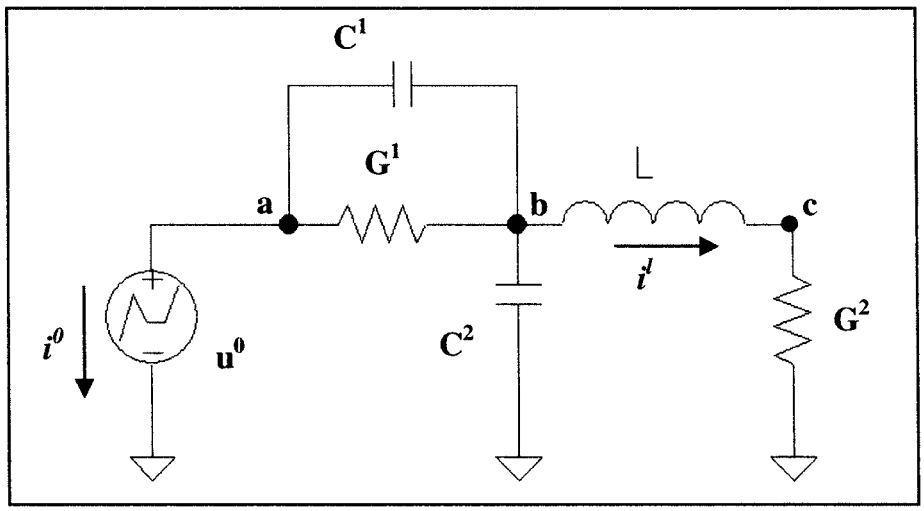

Fig. 4. RCL circuit.

$$
\begin{array}{c}
\begin{matrix} v^a & v^b & v^c & i^l & i^0 \end{matrix} \\
\begin{bmatrix} C^1 & -C^1 & 0 & 0 & 0 \\ -C^1 & C^1+C^2 & 0 & 0 & 0 \\ 0 & 0 & 0 & 0 & 0 \\ 0 & 0 & 0 & L & 0 \\ 0 & 0 & 0 & 0 & 0 \end{bmatrix}
\begin{bmatrix} \dot{v}^a \\ \dot{v}^b \\ \dot{v}^c \\ \dot{i}^l \\ \dot{i}^0 \end{bmatrix}
= -
\begin{bmatrix} G^1 & -G^1 & 0 & 0 & 1 \\ -G^1 & G^1 & 0 & 1 & 0 \\ 0 & 0 & G^2 & -1 & 0 \\ 0 & -1 & 1 & 0 & 0 \\ -1 & 0 & 0 & 0 & 0 \end{bmatrix}
\begin{bmatrix} v^a \\ v^b \\ v^c \\ i^l \\ i^0 \end{bmatrix}
+
\begin{bmatrix} 0 \\ 0 \\ 0 \\ 0 \\ -1 \end{bmatrix}
\begin{bmatrix} u^0 \end{bmatrix} \\
\mathbf{M} \quad . \quad \dot{x} \quad = - \quad \mathbf{R} \quad . \quad x \quad + \quad \mathbf{B} \; . \; u
\end{array}
$$

Fig. 5. MNA representation for circuit in Fig. 4.

The derivation of the templates for R, L and C elements is straightforward:

For the capacitors, C:

$$\mathbf{M} = \begin{matrix} v^a \\ v^b \end{matrix} \begin{bmatrix} C & -C \\ -C & C \end{bmatrix} \begin{matrix} v^a \\ v^b \end{matrix}$$

$$\mathbf{R} = [\mathbf{0}]$$

$$\mathbf{B} = [\mathbf{0}]$$

For the resistors, R:

$$\mathbf{M} = [\mathbf{0}]$$

$$\mathbf{R} = \begin{matrix} v^a & v^b \end{matrix} \begin{bmatrix} G & -G \\ -G & G \end{bmatrix} \begin{matrix} v^a \\ v^b \end{matrix}$$

$$\mathbf{B} = [\mathbf{0}]$$

For the inductors, L:

$$\mathbf{M} = \begin{matrix} v^a & v^b & i^l \end{matrix} \begin{bmatrix} 0 & 0 & 0 \\ 0 & 0 & 0 \\ 0 & 0 & L \end{bmatrix} \begin{matrix} v^a \\ v^b \\ i^l \end{matrix}$$

$$\mathbf{R} = \begin{matrix} v^a & v^b & i^l \end{matrix} \begin{bmatrix} 0 & 0 & 1 \\ 0 & 0 & -1 \\ -1 & 1 & 0 \end{bmatrix} \begin{matrix} v^a \\ v^b \\ i^l \end{matrix}$$

$$\mathbf{B} = [\mathbf{0}]$$

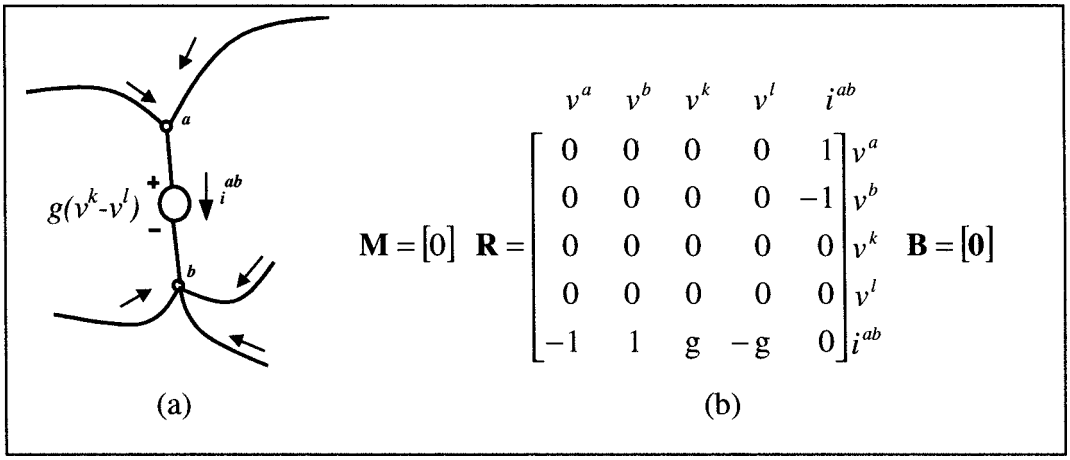

Fig. 6. (a) Voltage dependent-voltage source. (b) MNA template

In these example templates, and the rest of the examples in this section, the relative indices (v^a, v^b) are added for clarification purposes. Returning to Fig. 4 and putting these templates together, using the common shared node indices (a, b, c), gives the result shown in Fig. 5.

Mapping of Active Elements to the MNA

Active elements, such as independent sources, and dependent, controlled sources, require a different treatment for the creation of the corresponding templates. To exemplify this procedure, the development of the template for a voltage controlled voltage source follows.

Fig. 6(a) illustrates the general situation where a dependent voltage source is located between the nodes a and b of a network. We assume that the value of this source is controlled by the voltage difference between two different nodes of the circuit, k and l ($v^k - v^l$). The quantity g, which is the transconductance between the nodes k-l and a-b, acts as the proportionality parameter for the source. i^{ab} is the current through the controlled source measured from node a to b. A positive sign for currents leaving the node has been assumed.

Applying KCL to nodes a and b and using the definition of the control variable allows us to extract a template for this element of the form shown in Fig. 6(b).

This section has explained the mapping of active and passive devices onto the MNA matrix. The mapping for non-linear elements will be shown later in Section 4 through an example.

3.2. Time Domain Evaluation Formulation

In our technique, time evaluation of the PWL model is accomplished through an inverse Laplace evaluation approach, due to the benefits that this methodology offers. This technique consists of solving the system in the frequency domain and then using the inverse Laplace transform to obtain the time domain response. Inverse Laplace evaluation techniques are applicable to stiff systems and can perform well even when the system is in the presence of discontinuities in the functions [31]. Additionally, the methodology is robust to inconsistent initial condition situations. These properties result in stable techniques that do not face many of the convergence problems that affect the direct evaluation techniques.

Frequency Domain Analysis for Arbitrary Inputs

The following procedure was inspired by a similar development applied to a more specific system in [27].

Applying the Laplace transformation to the equations in Fig. 3, considering $x(0)$ to be the known initial conditions of the state vector x, and rearranging terms:

$$X(s) = (\mathbf{M}s + \mathbf{R})^{-1}\mathbf{B}U(s) + (\mathbf{M}s + \mathbf{R})^{-1}\mathbf{M}x(0), \tag{2}$$

Using the identity $\mathbf{R}\mathbf{R}^{-1} = \mathbf{I}$, where $\mathbf{I}$ is the identity matrix, and matrix algebra, we can rearrange the previous expression to be:

$$X(s) = (\mathbf{I} - s\mathbf{A})^{-1}\mathbf{T}U(s) - (\mathbf{I} - s\mathbf{A})^{-1}\mathbf{A}x(0), \tag{3}$$

where $\mathbf{A} = -\mathbf{R}^{-1}\mathbf{M}$ and $\mathbf{T} = \mathbf{R}^{-1}\mathbf{B}$.

Considering $\mathbf{A}$ diagonalizable, then $\mathbf{A} = \mathbf{K}\mathbf{\Lambda}\mathbf{K}^{-1}$. Where $\mathbf{\Lambda}$ is a diagonal matrix whose elements are the eigenvalues of $\mathbf{A}$ and $\mathbf{K}$ is the corresponding eigenvector matrix. Making this substitution into the previous expression and rearranging with matrix transformations allows one to obtain,

$$X(s) = \mathbf{K}(\mathbf{I} - s\mathbf{\Lambda})^{-1}\mathbf{g}U(s) - \mathbf{K}(\mathbf{I} - s\mathbf{\Lambda})^{-1}\mathbf{h}x(0), \tag{4}$$

where we use the following substitutions: $\mathbf{g} = \mathbf{K}^{-1}\mathbf{T}$ and $\mathbf{h} = \mathbf{K}^{-1}\mathbf{A}$.

It is straightforward to verify that the solution of the previous expression is of the form:

$$X(s) = \mathbf{Tr}(s)U(s) - \mathbf{Tri}(s)x(0), \tag{5}$$

where $\mathbf{Tr}(s)$ and $\mathbf{Tri}(s)$ are matrices whose structures obey the following formation rule:

$$X(s)_i = \sum_{j}^{size(U)} \left(\left(\sum_{k}^{row(g)} \frac{\mathbf{K}_{i,k} \cdot g_{k,j}}{1 - s \cdot \lambda_k} \right) U_j - \sum_{k}^{row(g)} \left(\frac{\mathbf{K}_{i,k} \cdot h_{kj}}{1 - s \cdot \lambda_k} \right) x(0)_j \right); \tag{6}$$

This is a direct solution in the frequency domain of the system for the state variable vector $X(s)$ under excitation $U(s)$ and initial conditions defined by the vector $x(0)$.

When the range of $\mathbf{A}$, corresponding to the number of nodes in the network, reaches several hundred, the computational task of solving the eigenvalue problem becomes very expensive. Alternative methods should be considered under these circumstances to evaluate the eigenvalues or natural frequencies of the system. Fortunately, in recent years, order reduction methods based on momentum matching or Padé approximation have been developed to efficiently solve very large linear problems [27–30]. The idea is to approximate the Laplace transfer function of the very large circuit to the response of a reduced-order model. These methods can be incorporated with few modifications into the present development because they are Transfer Laplace methods for the time-domain evaluation of networks.

After finding the frequency domain response of the network to a general input, the next step is to use this result as the basis from which to derive the time domain expression.

Time Domain Analysis

To overcome the computationally intensive task of an integration process in the time domain when a general excitation, $u(t)$, is considered, the inputs to the network are characterized using a piecewise linear approximation. Restricting the type of signals in the system to be PWL gives us an explicit time domain conversion expression that simplifies the evaluation algorithm.

The input to the system $u(t)$ in the period (t_{n-1}, t_n) can be approximated using:

$$u(t) \cong b_{n-1} + (b_n - b_{n-1})\frac{t}{(t_n - t_{n-1})} = b_{n-1} + \left[\frac{\Delta b}{T}\right] t, \tag{7}$$

where T is the sampling period and b_{n-1}, b_n represents the vector of inputs to the system for the timesteps t_{n-1} and t_n.

The response in an interval (t_{n-1}, t_n) for a linear time-invariant network, equation (6), under a general piecewise signal, equation (7), and with initial conditions different from zero will be:

$$x(t)_i = \sum_{j}^{size(u)} \left(\begin{array}{l} \left(b_{j_{n-1}} + \frac{\Delta b_j}{T}(t - t_{n-1})\right) \sum_{k}^{N} Tu(i,j,k) + \\ \sum_{k}^{N} Tu(i,j,k)\left(\left(b_{j_{n-1}} + \frac{\Delta b_j}{T}\lambda_k\right)\left(1 - e^{(t-t_{n-1})/\lambda_k}\right) - b_{j_{n-1}}\right)\Big|_{\lambda_k \neq 0} \end{array} \right) + \sum_{j}^{N} \left[\left(\sum_{k}^{N} \left(\frac{Tx(i,j,k)e^{(t-t_{n-1})/\lambda_k}}{\lambda_k} \right)_{\lambda_k \neq 0} - \sum_{k}^{N} Tx(i,j,k)\delta(t)\Big|_{\lambda_k = 0} \right) x(t_{n-1})_j \right]; \tag{8}$$

where:

$$Tu(i,j,k) = K_{i,k} \cdot g_{k,j};$$
$$Tx(i,j,k) = K_{i,k} \cdot h_{k,j};$$

$x(t)$ is the time response of the analysis. The expression has been shifted in time to be applicable to any general interval. Given that the time analysis is complete, we move onto determining the technique used to

switch between the different linear regions of a non-linear system.

3.3. Switching between PWL Models

The structure of the circuit network under simulation, and consequently its behavior, is characterized by its global mathematical representation as described in Section 3.1. The linear components in the network are completely characterized by a unique matrix representation. The non-linear elements, on the other hand, require multiple PWL models to represent their behavior. The simulation algorithm must select the proper PWL model for every non-linear device in the network according to their region of operation.

The switching between different models for a non-linear element depends on the state values (voltages) of the nodes corresponding to the inputs and outputs of the element. Consequently, during a simulation run, the switching of models for the nonlinear elements could and will occur as a response to the propagation of the input signal through the system to the output. A switching algorithm must determine the current region of operation for the device, and consequently use the proper PWL model.

The region of operation of non-linear devices is defined according to a set of conditions. The simplest of these conditions being a threshold level at the input port of the device that determines the boundary between two regions. The more general representation consists of an inequality equation that relates the values at the input and output ports of the device that defines a dynamic boundary between regions. Based on the way the switching algorithm employs these boundary conditions to select which PWL model to apply, two different approaches can be used. We have currently implemented a simple *Reactive Switching Approach* in Chatoyant, which finds the occurrence of switching between models for the non-linear devices by performing a check after each timestep. After an evaluation of the 'states' in the system, a test over the boundary conditions is performed. If the boundary conditions identify a region of operation different from the one corresponding to the PWL model currently in use, a change of models takes place. This action, consequently, will force the PWL simulator to re-compute the transfer function of the system since the global MNA representation has been altered.

The advantage of this method is the simplicity of implementation. However, there are drawbacks in the form of undesirable situations that can occur during the evaluation. It is possible for the simulator to choose a change that moves the current 'state' of the system to a transitory point where it takes many additional changes to get to the right 'state.' Even worse, it is possible to put the system into an erroneous condition that does not correspond to any true behavior of the circuit. These situations can be addressed by increasing the sampling rate for the PWL characterization and by guaranteeing continuity between PWL models.

We have also developed the theory for performing a *Predictive Switching Approach*. Instead of continuously checking for any switching occurrence, this approach predicts when the switch will take place, if the present input is maintained. Explicitly finding the time for the switching of regions involves the interaction of the inequality equations, which determine the regions of operation, and the transfer function of the system.

In general a switching condition in a device is given by a boundary condition of the form:

$$x_{in}(t) < f(x_{out}, V_{th}, t); \tag{9}$$

Where the state at the input port of the device $x_{in}(t)$ is checked against a function f on its output state, $x_{out}(t)$, and a fixed parameter V_{th}, that we call a threshold.

However, if the expression of $x(t)$ is known, the inequality can be transformed in an equation that defined the time of transition between regions, which is the desired switching time.

$$f(x_{out}, V_{th}, t_b) - x_{in}(t_b) = 0; \tag{10}$$

t is equal to the switching time t_b, when the expression (9) is converted to an equality. The equation (10) together with the expression for $x(t)$, equation (8), form a complete set of equations for the solution of the unknown t_b. This problem can be solved using traditional iterative methods for the general case of dealing with non-linear equations.

However for the purpose of establishing the principle behind the technique, we consider a simple linear relationship for the boundary condition, such as:

$$a \cdot x_{out}(t) + bV_{th} < x_{in}(t);$$

which, solving for t_b is:

$$a \cdot x_{out}(t_b) + bV_{th} = x_{in}(t_b); \tag{11}$$

The expression for $x(t)$, can be simplified if one only considers the steady state response to the input. That is, the time of the state evaluation is considered to

be long compared to the time of the transient response. Additionally, we consider that only non-zero eigenvalues are present. This represents the worst case scenario, since in this case the expression depends on more nonlinear terms (i.e., the exponential in the expression). With these considerations, $x(t)$ is given by:

$$x_i(t) = \sum_{j=1}^{N}\sum_{k=1}^{N}(T(i,j,k) \times [(b_{n-1} + S_{n-1}\lambda_k)(1 - e^{t/\lambda_k}) + S_{n-1}t]); \tag{12}$$

where the input to the system is given by the piecewise linear expression:

$$u(t) = b_{n-1} + S_{n-1}t;$$

Using expression (12) in expression (11) with some algebraic simplification gives:

$$\sum_{j=1}^{N}\sum_{k=1}^{N}(b_{n-1} + S_{n-1}\lambda_k)\, e^{t_b/\lambda_k}(T(in,j,k) - a \cdot T(out,j,k)) + \gamma \cdot S_{n-1}t_b + bV_{th} + \eta = 0 \tag{13}$$

where, the following substitutions were made:

$$\gamma = \sum_{j=1}^{N}\sum_{k=1}^{N}(a \cdot T(out,j,k) - T(in,j,k));$$

$$\eta = \sum_{j=1}^{N}\sum_{k=1}^{N}[(a \cdot T(out,j,k) - T(in,j,k)) \times (b_{n-1} + S_{n-1}\lambda_k)]$$

In expression (13), *in* represents the index of the input port and *out* the index of the output port. This expression can be further simplified using the following substitutions:

$$\theta = bV_{th} + \eta;\ \psi = \gamma S_{n-1};$$

$$\xi(in, out, j, k, b_{n-1}, S_{n-1}) = (b_{n-1} + S_{n-1}\lambda_k)(T(in,j,k) - a \cdot T(out,j,k));$$

$$\Gamma(k) = \sum_{j=1}^{N}\xi(j,k);$$

This gives:

$$\sum_{k}^{N}\Gamma(k)\, e^{t_b/\lambda_k} + \psi t_b + \theta = 0; \tag{14}$$

This expression is, in general, not analytically solvable. To obtain the desired values of t_b, or roots for the expression, an algorithm such as Newton-Raphson can be used. There is, however, an important consideration that can be used to simplify the task. The exponential terms in expression (14) are affected by the relation t_b/λ_k. Consequently the value of λ_k can be considered as a time constant for the devices in the system. If the input sample time is small compared to λ_k, the resulting exponential expression can be considered constant during this period of time. Consequently, if the period of the incoming piecewise signal t_i is much less than the time constant of the resonant frequency considered $(1/\lambda_k)$ then this term could be considered constant for the evaluation of t_b.

$$\text{if } \lambda_h \gg t_i \Rightarrow \lambda_h \gg t_b \Rightarrow e^{t_b/\lambda_h} \cong t_b/\lambda_h + 1$$

$$\sum_{k}^{N-d}\Gamma(k)\, e^{t_b/\lambda_k} + (\psi + \Psi)t_b + \varphi = 0; \tag{15}$$

$$\text{using} \quad \Psi = \sum_{k}^{d}\frac{\Gamma(k)}{\lambda_h};\ \varphi = \theta + \sum_{k}^{d}\Gamma(k)$$

In the final expression, (15), the number of possible roots of t_b is decreased to $N - d$, where d is the number of time constants that are much larger than the input time period. The fact that the domain for the roots is restricted to be in the interval $(0, t_i)$ also simplifies the computation task. This is because the iterative algorithm used to solve it will have fixed boundaries for the search for the roots.

Once the switching time for the device is determined, then a comparison against the time range of the input signal can be performed. It is important to remember that the validity of the calculated switching time is tied to the PWL input signal. Consequently, any switching times that fall outside the time range of the input signal must be discarded.

Using this technique, the validated switching time and the corresponding device are then scheduled in an event list that can be used as the basis for a "switching scheduler." During the evaluation period, only the scheduler's list is checked for any switching event that can occur during its timestep. If any switching event is found, the MNA modification takes place and recomputation of the global transfer function is performed. The scheduler list must then be cleared since it is no longer valid. Then, the prediction algorithm must be re-run to generate a new list.

This switching methodology would be very fast and its implementation in our tool is a subject for future work. However, we now return to examples of the modeling of devices using our PWL modeling technique.

4. Optoelectronic Modeling: VCSEL Example

To show the application of PWL techniques to the modeling of optoelectronic components, the modeling of one of the more promising devices in this area is now presented. This section also describes how we map non-linear elements into the MNA matrix.

Vertical cavity surface emitting lasers (VCSEL) are semiconductor devices that have the ability to emit and modulate coherent light under electrical excitation. The optical cavities of these devices are orthogonal to their surface, which allows their optical output to be perpendicular to the surface of the chip. This property allows one to fabricate these devices in a two dimensional array which greatly increases the communication bandwidth of the resulting optical element. It is the advantage of having multiple laser channels on the same chip that makes this technology so attractive. Consequently, VCSELs have become the optical source of choice for almost every optoelectronic link currently designed [33,34].

Typical L-I and V-I diagrams for a VCSEL are shown in Fig. 7(a) [34]. The segmented curve represents the relation between voltage and current in the device, and the solid curve is the relation between the optical power generated by the VCSEL versus the electrical current consumed.

PWL Modeling of the L-I Characteristics The optical output of VCSEL devices is a non-linear function, as can been seen in Fig. 7(a). The current in the laser must exceed a threshold value to begin the lasing process. After this, the optical power production reaches a maximum value and then decreases with further increases in electrical current. The reason for this behavior is the loss of efficiency in the laser, caused by the increase in temperature as a consequence of the ohmic losses [36].

To model this behavior of the device, however, is typically challenging because the optical power is not an electrical parameter. Nevertheless, an interesting feature of the PWL methodology is that it is not tied only to the electrical domain, as the PWL technique can be used to model signals that cross different domains. A characterization of the optical power variable is possible in this method by its inclusion into the MNA as an unknown term to be evaluated. The VCSEL device is then seen by the simulator framework as a black box, which has two ports: the input electrical port and the output optical port. Fig. 8 illustrates this concept.

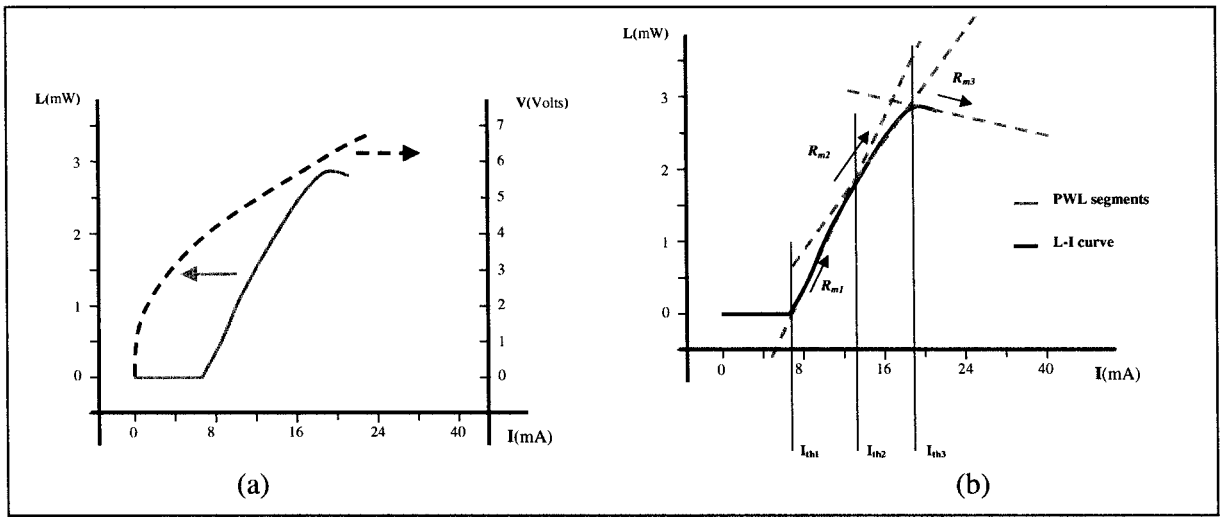

Fig. 7. (a) L-I and V-I curves for a VCSEL[35] (b) L-I curve with PWL model functions.

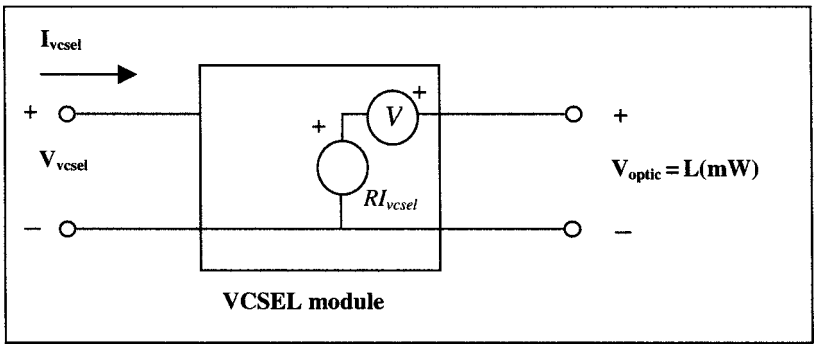

Fig. 8. System-level simulator VCSEL model.

For the MNA mathematical representation, the optical behavior is simply an additional port that depends on a state variable parameter in a different location in the network. To create the template for this behavior, the equivalence between the optical power parameter L and a voltage type variable in the network V_{optic} is established.

Fig. 7(b) shows the L-I curve and a possible choice of three linear segments to fit the curve. These linear functions are partitioned into regions by the threshold currents I_{th1}, I_{th2}, and I_{th3}.

The mathematical definition of the PWL models for the optical behavior of the VCSEL using these regions of operation is given by:

$$V_{optical} = \begin{cases} R_{m3}I - V_3 & I > I_{th3}, \\ R_{m2}I - V_2 & I_{th2} < I < I_{th3}, \\ Rm_{m1}I - V_1 & I_{th1} < I < I_{th2}, \\ 0 & I < I_{th1}, \end{cases}$$

$$V_1 = R_{m1}I_{th1},$$
$$V_2 = R_{m2}I_{th2} - R_{m1}(I_{th2} - I_{th1}),$$
$$V_3 = R_{m3}I_{th3} - R_{m2}(I_{th3} - I_{th2}) - R_{m1}(I_{th2} - I_{th1}),$$

The values of V_3, V_2, and V_1 are necessary for continuity and the threshold values correspond to the chosen points for the curve fitting process.

The PWL template for each of the regions of operation share the same generic form:

$$\begin{array}{cc} & \begin{array}{ccccc} v^{optical} & v^x & i^v & i^c & i^{vcsel} \end{array} \\ \mathbf{M} = [\mathbf{0}] \quad \mathbf{R} = & \left[\begin{array}{ccccc} 1 & 0 & 1 & 0 & 0 \\ 0 & 0 & -1 & 1 & 0 \\ -1 & 1 & 0 & 0 & 0 \\ 0 & -1 & 0 & 0 & \mathrm{R}_m \\ 0 & 0 & 0 & 0 & 0 \end{array}\right] \begin{array}{c} v^{optical} \\ v^x \\ i^v \\ i^c \\ i^{vcsel} \end{array} \end{array}$$

$$\mathbf{B} = [0 \quad 0 \quad -V \quad 0 \quad 0]i^v$$

R_m and V correspond to the pair (R_{m1}, V_1) for region 1, (R_{m2}, V_2) for region 2, and (R_{m3}, V_3) for region 3. Indexes v^x, i^v, i^c are auxiliary indexes to form the template. The terminal $v^{optical}$ refers to the optical output and the terminal i^{vcsel} the controlling current from the input port.

The advantage of this characterization is that the designer can directly simulate the effect of electrical conditions in the VCSEL or associated driver circuit against the optical power produced by this device. Additional variable dependencies can be added to the L-I VCSEL model following this approach (e.g., temperature, spot size, and threshold) that allow one to study their effect on complete systems. As shown in [37], this VCSEL model is used to examine the dependency of BER on the temperature at which the device is operated.

For the complete modeling of the VCSEL, the same technique is also used for additional non-linear characteristics, such as the V-I curve. This is presented in [37] and is not included here for space considerations.

5. Micro Mechanical Modeling

In the field of MEM modeling, there has been an increasing amount of work that uses a set of Ordinary Differential Equations to characterize MEM devices [11,38,39]. ODE modeling is used instead of techniques such as finite element analysis, to reduce the time and amount of computational resources necessary for simulation. The model uses non-linear differential equations in multiple degrees of freedom and in mixed domains. The technique models a MEM device by characterizing its different basic components such as beams, plate-masses, joints, and electrostatic gaps, and by using local interactions between components.

The general module for solving sets of non-linear differential equations using piecewise linear techniques can be used to integrate complex mechanical models into our design tool. The model for a mechanical device can be summarized as a set of differential equations that define its dynamics as a reaction to external forces. This model must then be converted to the same form as in the electrical case to be given to the PWL solver for evaluation. We explain this technique next.

With damping forces proportional to the velocity, the equation of motion for a mechanical structure with viscous damping effects is [40]:

$$F = \mathbf{K}U + \mathbf{B}V + \mathbf{M}A \tag{16}$$

where, $\mathbf{K}$ is the stiffness matrix, U is the displacement vector, $\mathbf{B}$ is the damping matrix, V is the velocity vector, $\mathbf{M}$ is the mass matrix, A is the acceleration vector, and F is the vector of external forces affecting the structure. Obviously, knowing that the velocity is the first derivative and the acceleration is the second derivative of the displacement, the above equation can be recast to:

$$F = \mathbf{K}U + \mathbf{B}U' + \mathbf{M}U'' \tag{17}$$

Similar to the electrical modeling case, this equation represents a set of linear ODEs if the characteristic matrices $\mathbf{K}$, $\mathbf{B}$, and $\mathbf{M}$ are static and independent of the dynamics in the body. If the matrixes are not static and independent (e.g., the case of aerodynamic load effects), they represent a set of non-linear ODEs.

To reduce the above equation to a standard form, we use a modification of Duncan's reduction technique for vibration analysis in damped structural systems [41]. This modification allows the above general mechanical motion equation to be reduced to a standard first order form, similar to electrical equation found in Fig. 3. This gives a complete characterization of a mechanical system.

$$\begin{bmatrix} \mathbf{0} & \mathbf{M} \\ \mathbf{M} & \mathbf{B} \end{bmatrix} \begin{bmatrix} U'' \\ U' \end{bmatrix} + \begin{bmatrix} -\mathbf{M} & \mathbf{0} \\ \mathbf{0} & \mathbf{K} \end{bmatrix} \begin{bmatrix} U' \\ U \end{bmatrix} = \begin{bmatrix} \mathbf{0} \\ \mathbf{I} \end{bmatrix} F \tag{18}$$

Using substitutions, equation (18) is rewritten as:

$$\mathbf{Mb}X' + \mathbf{Mk}X = \mathbf{E}F,$$

where the new state variable vector

$$X = \begin{bmatrix} U' \\ U \end{bmatrix} \tag{19}$$

Each mechanical element (beam, plate, etc.) is characterized by a template consisting of the set of matrices **Mb** and **Mk**, composed of matrices $\mathbf{B}$, $\mathbf{M}$, and $\mathbf{K}$ in the specified form seen above. If the dimensional displacements are constrained to be small and the shear deformations are ignored, the derivation of **Mb** and **Mk** is simplified and independent of the state variables in the system. Multi-node idealization can be performed by combining basic elements (e.g., two nodes) to characterize higher order modes.

Typically, this element is only a part of a bigger device made from individual components that are characterized using similar expressions. The generalization of the previous case to an assembly of elements or mechanical structures is fairly straightforward. The general expression, seen in equation (19), characterizes the whole structure defined by a set of nodes, from which every individual element shares a subset. The next step, similar to the previously considered electronic case, is merging the individual templates together, composing the general matrix representation for the composed structure. However, a common coordinate reference must be used for this characterization of mechanical structures, since every template or element is characterized in a local reference system. The process of translation of these local templates to the global reference system can be described by [40]:

$$S = \mathbf{A}^T \overline{S} \mathbf{A} \tag{20}$$

where, $\mathbf{A}$ represents the translation matrix from local displacements to global displacements (a function of the structure's geometery), $\overline{S}$ represents the local template, and S is the corresponding global representation. The next step is the addition of these global representations into the general matrix form, using the matrices' nodal indexes as reference. Finally, the piecewise linear

solver can be used on the composed system's general matrix.

The general matrix representation of the system is constant if a linear behavior is considered; consequently the problem is reduced to the solution of a linear system as given by expression (8). Under these conditions, the PWL simulator operates efficiently using the PWL characterization of the signals to offer one pass integration evaluation. In a more general non-linear simulation general matrix representation changes according to different PWL templates in response to different regions of operation.

The use of a general PWL solver for mechanical simulation decreases the computational task and allows for a trade-off between accuracy and speed. The accuracy can be increased in both linear and non-linear situations using a more dense granularity for the PWL signal representation or by using a bigger set of PWL representations for non-linear behavior.

The additional advantage of using the same technique to characterize electrical and mechanical models allows us to easily merge both technologies in complex devices that interact in mixed domains.

As in electrical modeling, matrices for different mechanical components are required for our PWL modeling technique. In fact, the matrices, which compose the templates for the mechanical elements, have been already developed in the field of structural mechanics [40]. These matrices for individual basis elements are called equivalent matrices. They are discrete lumped abstractions of the real elements. An example of these mechanical component matrices are presented in the next section.

6. Simulated Results and Verification

In this section we evaluate the accuracy and speed of our PWL technique as well as its ability to integrate multiple domains in the same simulation framework. In order to test the speed and accuracy of our models, we performed several experiments comparing our results in the electrical domain to that of SPICE 3f4 (Level II). These experiments are presented in the first part of this section. The second part of this section illustrates mixed-domain simulation in a design framework, as we use Chatoyant to model a 2×2 optical MEM switch. For all these tests, the non-linear MOS transistors are modeled using a PWL characterization with 40 regions of operation [37].

6.1. Accuracy Comparison to an Analog Simulator

This test was the performance of a single CMOS inverter, fabricated in 0.5 μm technology, under large signal input. The source used for the test was a pure sinusoid where the frequency was varied to explore the dynamic range of the amplifier .

The number of samples for each period was fixed at 100 for the models. SPICE was set to give a division of the period of at least 100 samples. However, we note that the control for the number of convergence attempts in SPICE is automatic. A load was selected for the amplifier that matches the typical input capacitive load of a similar stage (6 fF). It is important to note that we used the static (zero bias) capacitance values directly from the SPICE level II models. Fitting the model equations to the dynamic behavior of the parasitic capacitances would decrease the relative error and additionally expand the region of validity for a fixed tolerance.

As a graphical representation of the behavior of the modeling technique, we show in Fig. 9 the response of the amplifier from SPICE simulations and from simulation using the PWL model at a frequency of 100 MHz. The curves for the response are almost on top of each other. The percentage of error between the responses is below 4% in the low to middle range frequencies (10–100 MHz) for the PWL model. In the high frequency range (1 GHz), not shown, the model suffers higher error rates due to the phase shift between the PWL and SPICE waveforms. This suggests the necessity of better parameter fitting for the parasitic capacitances in the model.

6.2. Speed Comparison to an Analog Simulator

A multistage experiment with a significant number of drivers was simulated to test the performance of our models. The sizes of the test circuits chosen were 48, 96, and 192 FETs. The experiments were conducted at 10, 100, 500, and 1000 MHz. For each experiment we simulated 10 periods of the operating frequency. To test dependence on the sampling rate, the number of timesteps requested of SPICE and required by our model were 50, 100, 200, and 400 for each period of the signal. For SPICE runs the number of timesteps used were very close to the number requested (within 1%). For the PWL algorithm this number is exactly the same, because it is enforced to be exactly what is requested.

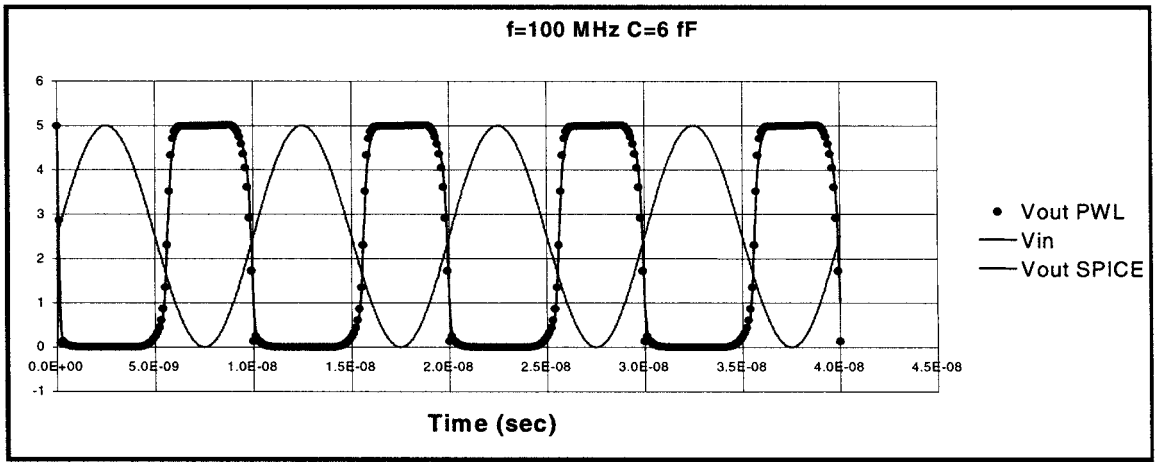

Fig. 9. PWL and SPICE output under capacitive load and frequency of 100 MHz.

Table 1 shows the performance of our models against SPICE for two of the example cases: 10 MHz and 1 GHz. The speed-up achieved for the same number of timesteps is at least two orders of magnitude. The increase in execution time vs. size of the circuit under test for SPICE is well known to be superlinear [42]. This behavior is evidenced in the time of execution used by the SPICE simulator to solve the three sizes of test circuits used in the experiment. On the other hand, each CMOS inverter is a separate model and the modules modeled using PWL are independently handled by the discrete event scheduler in Chatoyant [26]. Chatoyant's DE scheduler shows a high level of efficiency by maintaining a close to linear increase in execution time with an increase in circuit size.

When a simulator reacts to stiff signals (signals with slow variations compared to the natural frequencies), it loses efficiency due to the stability constraints imposed by the integration solution techniques. The stiffness problem is usually overcome by increasing the sampling rate, which increases the total execution time. The low frequency results seen in Table 1 shows the behavior of the PWL model under a high degree of stiffness.

Table 1. SPICE vs. PWL models in a system of multiple FETs.

	Times (secs) (4000 total timesteps)			
	SPICE		PWL	
Size (# of FETs)	$F = 10$ MHz	$f = 1$ GHz	$f = 10$ MHz	$f = 1$ GHz
48	54.39	36.22	4.62	1.23
96	184.01	64.64	6.38	2.05
192	556.54	302.85	11.95	3.19

In our case, stiffness imposes extra computation time in the eigenvalue solution and the PWL switching. Therefore, in both SPICE and our PWL models, the execution times is noticably higher under these conditions.

6.3. *Piecewise Linear Modeling of Mechanical Beams*

As an example of our mechanical modeling techniques, we present the response of an anchored beam in a 2D plane (x-y plane) with an external force applied on the free end. The template for the constrained beam is composed of the following matrices. These matrices are used in equations (18)–(20), in solving for the response of the beam. Note, the matrices are reduced with respect to the index associated at the anchored node.

$$\mathbf{K} = \frac{EI_z}{l^3}\begin{bmatrix} \dfrac{A\lambda^2}{I_z} & 0 & 0 \\ 0 & 12 & -61 \\ 0 & -61 & 4l^2 \end{bmatrix};$$

$$\mathbf{M} = \frac{\rho Al}{420}\begin{bmatrix} 140 & 0 & 0 \\ 0 & 156 & -221 \\ 0 & -221 & 4l^2 \end{bmatrix};$$

$$\mathbf{B} = \delta\begin{bmatrix} 1 & 0 & 0 \\ 0 & 1 & 0 \\ 0 & 0 & 0 \end{bmatrix};$$

The viscosity factor, δ, in the system is made to act over x and y components, which are the two degrees of freedom given to the system.

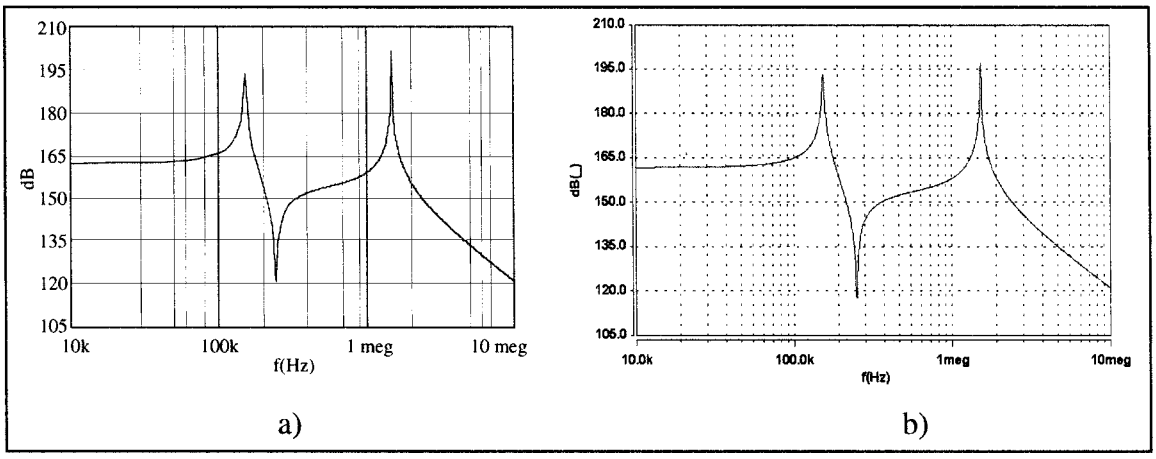

Fig. 10. Frequency response of a beam: (a) Chatoyand. (b) NODAS.

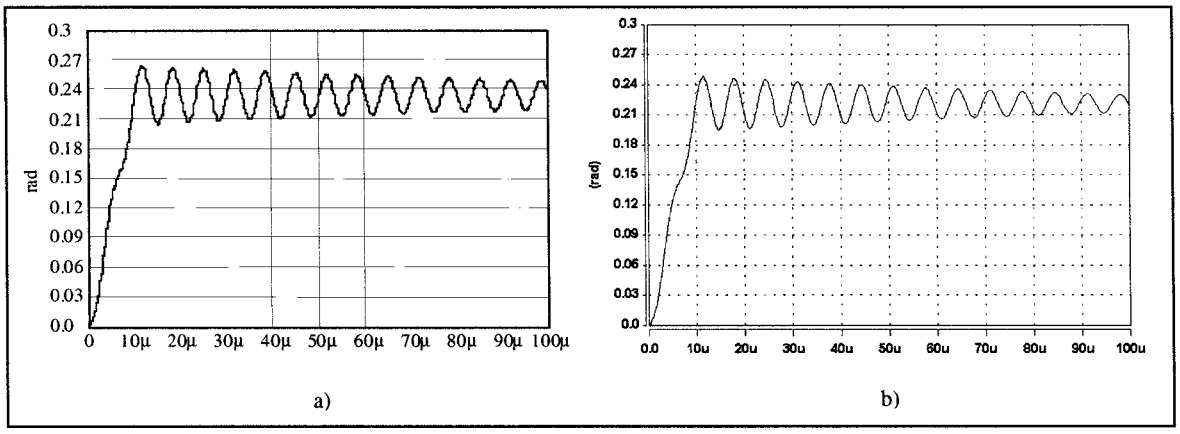

Fig. 11. Transient response of a beam: (a) Chatoyand. (b) NODAS.

To test our results, a comparison against NODAS [11] was performed. Fig. 10 shows the frequency response and corresponding resonant frequencies for this constrained beam (183 μm length, 3.8 μm width, poly-Si) from both our PWL technique and NODAS. The transient response to 1.8 nN non-ideal step (rise time of 10 μsec) rotational torque is also simulated. The rotational deformation to this force is shown in Fig. 11. As can be seen, the comparison between our results and NODAS's are very close. We also compare the resonant frequencies of the beam (simulated with 10 nodes) with Ansys [43]. The results for the first five resonant frequencies differ by less than 0.7%.

NODAS uses SABER, a circuit analyzer performing numerical integration for every point analyzed, which results in costly computation time. As mentioned earlier, our piecewise linear solver is computational intensive during the eigenvalue search, however, this procedure is performed only one time at the beginning of the simulation run. This results in a more computationally efficient simulation. However, the accuracy of the analysis depends in the granularity of the piecewise characterization for the signals used in the system, which can increase computation time.

6.4. Multi-Domain Simulation

To demostrate the modeling and simulation of mixed-domain systems in a single framework, we present

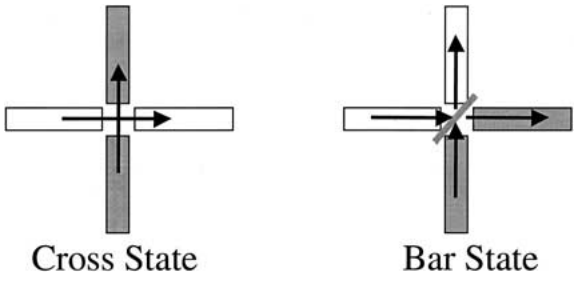

Fig. 12. 2×2 switch: cross and bar state.

the modeling and simulation of a 2×2 optical MEM switch. The general architecture of this switch consists of a set of four optical fibers in the shape of a "+" sign, with the input and output fibers facing each other through a free-space gap. The switching system is in the "cross" state when the light is passed straight across the free-space gap. However, to switch to the "bar" state, a micro- mirror is inserted between the fibers at a 45-degree angle, and the light is reflected to the alternate output. These two cases are shown in Fig. 12.

For the simulations presented in this paper, we use a switching system based on an experimental system designed and tested at UCLA [25]. Similar to that system, a mirror is placed on top of a long anchored cantilever beam. In our system, the bar state is achieved in the steady-state of the system, with the mirror positioned between the fibers in the free-space gap. The cross state is achieved by the cantilever beam bending towards the substrate, moving the attached mirror out of the optical path. The beam movement is a result of electrostatic attraction between a voltage applied below the cantilever and the beam itself. This attraction results in a force being applied to the beam

For simplicity, we simulate only a single input switching to either the cross or bar state throughout this example. A diagram of the system is shown in Fig. 13(a) with both output states represented by the solid and dashed arrows, respectively. Recall, the Chatoyant representation of this system is shown in Fig. 1. The mirror is 100×100 μm, and is positioned at the end of a 700 μm cantilever beam. Both beam and mirror are fabricated with polysilicon, with the mirror assumed to have an ideal reflectivity of 100%. The beam is 2 μm wide and 100 μm thick, while the mirror is 4 μm thick, to ensure the mirror remains rigid. The collimating lenses ($f = 50$ μm) are placed 50 μm from the fiber ends, and there is a free-space gap of 100 μm between the lenses. The mirror, when in the optical path, is positioned in the center of the free-space gap, 50 μm from each lens.

The modeling of the mechanical beam and electrostatic attraction is performed using the PWL technique described throughout this paper. Chatoyant's optical modeling technique is based on the Rayleigh-Sommerfeld scalar diffraction formulation [44]. We use RSoft's BeamPROP [45] to simulate the light through the fiber, and have developed an interface between

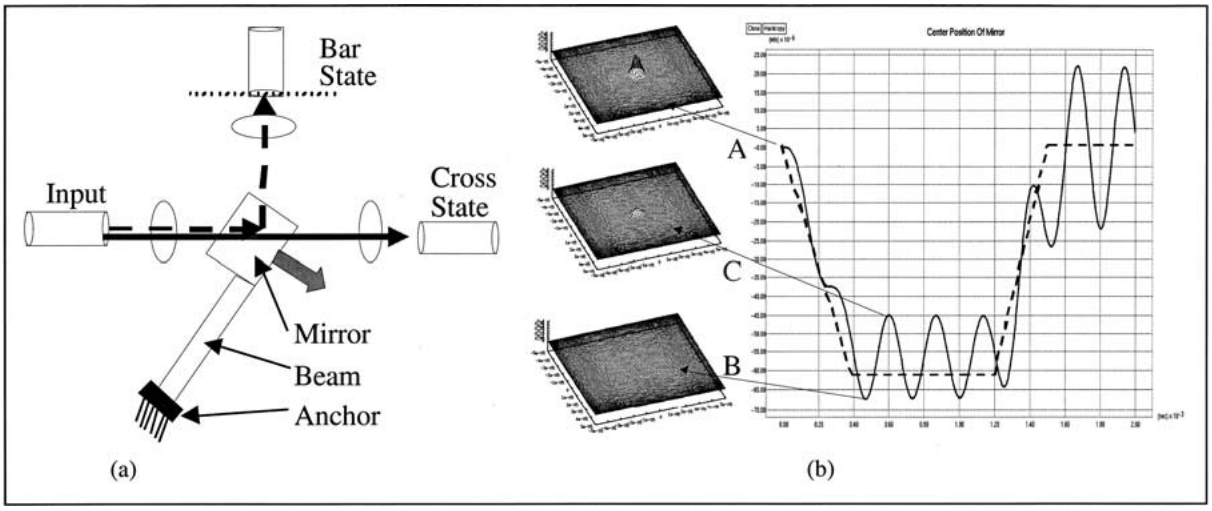

Fig. 13. (a) Switching system. (b) Mirror response and intensity distributions.

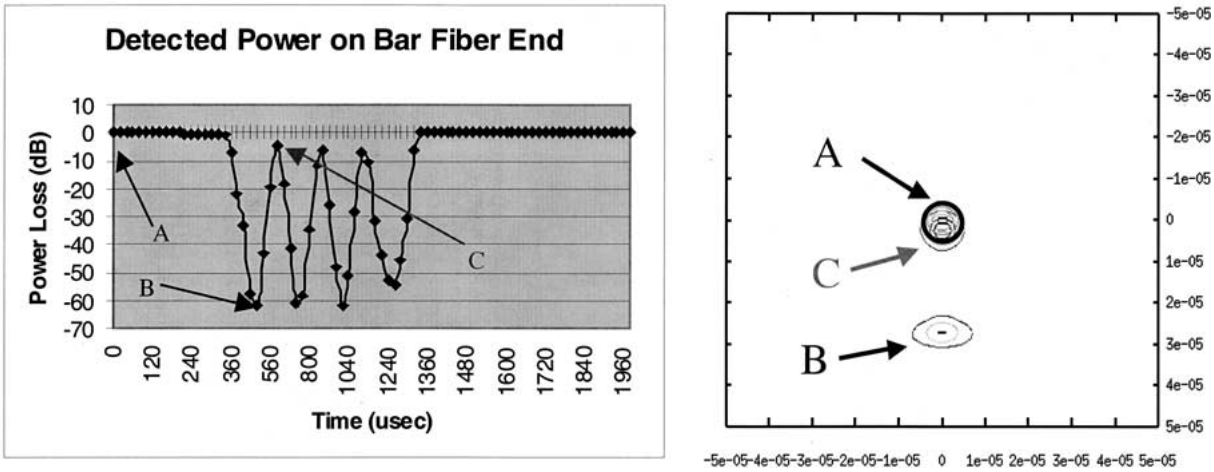

Fig. 14. (a) Power received on end of bar fiber. (b) Contour distributions.

the fiber propagation (BeamPROP) and free-space (Chatoyant) through a data file.

We first use Chatoyant to analyze the mechanical movement of the beam and mirror. The more significant mode frequencies of the beam, including the mirror mass, are determined to be 3.7 kHz and 27.1 kHz. These results are within 5% of the solution given from ANSYS. For a switching speed of 400 μsec, the response of the beam, in terms of the center position of the mirror from the original steady-state value, is shown in Fig. 13(b). The switching electro-static force applied to the cantilever beam is also included in Fig. 13(b), represented by the dashed line.

We next examine the optical power that is detected on a 100 μm square observation plane at the bar fiber. Optical intensity distributions at the observation plane are included for three points on the response curve, labeled A, B, and C. A is when the mirror is completely inserted in the optical path, achieving the bar state in the system. B is at the point where the mirror is totally out of the optical path, achieving the cross state. As seen in the intensity distribution, no substantial power reaches the bar fiber observation plane. As the mirror vibrates, because of the modal excitation, C is measured as the mirror partially moves back into the optical path, causing some light to be reflected off the mirror and be detected at the bar fiber. However, at this time, the switch is set in the cross state, causing the possibility of crosstalk or the detection of a false "1" on the bar fiber. This problem is further exemplified in Fig. 14(a). This shows a graph of the power detected on the bar fiber end (10 μm diameter) in terms of dB lost. As expected, the power detected corresponds to the mirror position movement seen in Fig. 13(b). During the mirror response, point C has a power loss of only 3 dB at the bar fiber end, resulting in 50% of the power still being detected at the bar fiber.

The three intensity contours for each of the points A, B, and C, are seen in Fig. 14(b), along with a circle drawn to represent the fiber end. For case A, the light strikes the mirror in the center and reflects directly into the bar fiber. As seen through Fig. 14(a) and (b), the contour for A is directly on the fiber, and we consider this full detected power (0 dB loss). For case B, the mirror is moved totally out of the optical path, resulting in virtually no power being detected on the fiber (61 dB of loss). However, it is interesting to note that even though almost no power is received at the fiber end, there is still a diffractive effect, with very low power, striking the observation plane, approximately 28 μm away from the fiber center. In a single channel system, it is not a problem, however, this effect could introduce crosstalk in larger scaled systems. For case C, when half the optical beams reflects off the mirror, the power is still concentrated, however, it is centered 3 μm from the fiber center, resulting in a 3 dB loss of power at the bar fiber end. We note that with a slower switching speed, the vibration is not significant, and the system experiences close to zero crosstalk.

7. Summary and Conclusions

We have presented a methodology for the simulation of mixed-technology (optical, electrical and mechanical) devices in a system-level simulation framework. The system simulation is a discrete event simulation of piecewise linear signals. However, each electrical or mechanical module in the system is itself a moderate sized non-linear network modeled using a Modified Nodal Analysis formulation and solver, with a switching algorithm to control the switching of regions of operation for the constituent non-linear devices. Unlike previous approaches, these networks are direct representations of the structure of modules without artificial switches or dummy components.

This modular representation, when used in a system-level approach with the addition of an efficient multi-domain simulator, can be used as a powerful tool for analysis in both the early and later stages of the design of multi-domain systems. This is because speed vs. accuracy trade-offs in simulation performance can be accomplished either with an increase in the number of PWL regions used to model non-linearity in the devices, or with an increase in the sampling rate of the signals in the system. Therefore, design space exploration can be done quickly with simple models, or coarse sampling rates. This can be followed with more accurate simulations based on detailed models and improved accuracy, all within the same simulation environment.

This same methodology, generalized with a formal mathematical definition of dynamic systems in any domain, allows for the integration of multiple domains in a single system. Consequently, additional domains could follow the same general methodology to increase the number of domains supported in a single mixed-technology CAD tool.

Acknowledgment

This work was supported by DARPA, under Grant No. F3602-97-2-0122 and NSF, under Grants No. ECS-9616879 and CCR-9988319.

References

1. Wu, M. C., "Micromachining for optical and optoelectronic systems," in *Proceedings of the IEEE* 85(11), pp. 1833–1856, November 1997.
2. CODE V is a registered trademark of Optical Research Associates, Inc.
3. Breault Research Organization, Inc., http://www.breault.com/.
4. Mukherjee, T. and Fedder, G. K., "Structured design of microelectromechanical systems," in *Proceedings of 34th Design Automation Conference,* Anaheim, CA, pp. 680–685, June 1997.
5. Coventor, Inc., http://www.coventor.com/
6. MEMSCAP, http://memscap.e-sip.com/
7. Jacquemod, G., Vuorinen, K., Gaffiot, F., Spisser, F., Seassal, C., Leclercq, J-L., Rojo-Romero, P. and Viktorovitch, P., "MOEMS modeling for opto-electro-mechanical co-simulation." *Journal of Modeling and Simulation of Microsystems* 1(1), pp. 39–48, 1999.
8. Morikuni, J. J., Mena, P. V., Harton, A. V. and Wyatt, K. W., "The mixed-technology modeling and simulation of optoelectronic microsystems." *Journal of Modeling and Simulation of Microsystems* 1(1), pp. 9–18, 1999.
9. Romanowicz, B., *Methodology for the Modeling and Simulation of Microsystems.* Kluwer Academic Publishers, Norwell, Massachusetts, pp. 24–39, 1998.
10. Yang, A. T. and Kang, S. M., "iSMILE: A novel circuit simulation program with emphasis on new device model development," in *Proceeding of the 26th ACM/IEEE Design Automation Conference,* pp. 630–633, 1989.
11. Morikuni, J. and Kang, S., *Computer-Aided Design of Optoelectronic Integrated Circuits and Systems.* Prentice-Hall, Inc., New Jersey, Chapter 2 and 6, 1997.
12. Vandemeer, J. E., "Nodal design of actuators and sensors (NODAS)." M.S. Thesis, Department of Electrical and Computer Engineering, Carniege Mellon University, Pittsburgh, PA, 1997 (unpublished).
13. Gupta, R. K., Hung, E. S., Yang, Y. J., Ananthasuresh, G. K. and Senturia, S. D., "Pull-in dynamics of electrostatically-actuated beams," in *Proc. Solid-State Sensor & Actuator Workshop,* June 1996.
14. Ananthasuresh, G. K., Gupta, R. K. and Senturia, S. D., "An approach to macromodeling of MEMS for nonlinear dynamic simulation," in *ASME'96 International Mechanical Engineering Congress and Exposition, Proc. of Dynamics Systems and Controls,* DSC-59, Atlanta, pp. 401–407, November 1996.
15. Kielowski, R., *Inside SPICE: Overcoming the Obstacles of Circuit Simulation.* McGraw-Hill, Inc., New York, Chapter 1 and 3, 1994.
16. Kao, R. and Horowitz, M., "Timing analysis for piecewise linear rsim." *IEEE Trans. Computer-Aided Design* 13(12), pp. 1498–1512, 1994.
17. Salz, A. and Horowitz, M., "IRSIM: An incremental MOS switch-level simulator," in *Proceedings of the 26th Design Automation Conference,* pp. 173–178, 1989.
18. Kawakita, K. and Ohtsuki, T., "NECTAR 2 a circuit analysis program based on piecewise linear approach," in *Proceedings of ISCAS,* Boston, pp. 92–95, 1975.
19. Zaman, M. H., Bart, S. F., Gilbert, J. R., Swart, N. R. and Mariappan, M., "An environment for design and modeling of electro-mechanical micro-systems," *Journal of Modeling and Simulation of Microsystems* 1(1), pp. 65–76, 1999.
20. Leenaerts, D. M. W. and Bokhoven, W. M. G., *Piecewise Linear Modeling and Analysis.* Kluwer Academic Publishers, Boston, Chapter 4, 1998.

21. Vandeberghe, L., Moor, B. De and Vandewalle, J., "The generalized linear complementary problem applied to the complete analysis of resistive piecewise linear circuits." *IEEE Trans. Circuits and Systems* 36, pp. 1382–1391, 1989.
22. Yamamura, K. and Ochiai, M., "An efficient algorithm for finding all solutions of piecewise-linear resistive circuits." *IEEE Trans. Circuits and Systems* 39, pp. 213–221, 1992.
23. Pejovic, P. and Maksimovic, D., "An algorithm for solving piecewise linear networks that include elements with discontinuities characteristics." *IEEE Trans. Circuits and Systems* 43, pp. 453–460, 1996.
24. Levitan, S. P., Kurzweg, T. P., Marchand, P. J., Rampel, M. A., Chiarulli, D. M., Martinez, J. A., Bridgen, J. M., Fan, C. and McCormick, F. B., "Chatoyant: A computer-aided-design tool for free-space optoelectronic systems." *Applied Optics* 26, pp. 6078–6092, September 1998.
25. Chen, R. T., Nguyen, H. and Wu, M. C., "A high-speed low-voltage stress-induced micromachined 2×2 optical switch." *IEEE Photonics Technology Letters* 11(11), pp. 1396–1398, November 1999.
26. Buck, J., Ha, S., Lee, E. A. and Messerschmitt, D., "Ptolemy: A framework for simulating and prototyping heterogeneous systems." *Int. J. Comput. Simulation* 4, pp. 155–182, 1994.
27. Feldmann, P. and Freund, R. W., "Efficient linear circuit analysis by Padé approximation via the Lanczos process." *IEEE Trans. Computer-Aided Design* 14, pp. 639–649, May 1995.
28. Pillage, L. T. and Rohrer, R. A., "Asymptotic waveform evaluation for timing analysis." *IEEE Trans. Computer-Aided Design* 9, pp. 352–366, April 1990.
29. Odabasioglu, A., Celik, M. and Pileggi, L. T., "PRIMA: Passive reduced-order interconnect macromodeling algorithm." *IEEE Trans. Computer-Aided Design* 17(8), pp. 645–654, 1998.
30. Kim, S., Gopal, N. and Pillage, L. T., "Time-domain macromodels for VLSI interconnect analysis." *IEEE Tran. on CAD of Integrated Circuits and Systems* 13(10), pp. 1257–1270, October 1994.
31. Vlach, J. and Singhal, K., *Computer Methods for Circuit Analysis and Design.* Van Nostrand Reinhold, New York, NY, Chapters 4 and 12, 1994.
32. Freund, R. W. and Feldmann, P., "Reduced-order modeling of large passive linear circuits by means of the SyPVL Algorithm," in *Proceedings of the ICCAD,* pp. 280–217, November 1996.
33. Kibar, O., "VCSEL-based digital free-space optoelectronic interconnections." Ph.D. Dissertation, University of California, San Diego, 1999 (unpublished).
34. Fan, C., Mansoorian, B., Van Blerkom, D. A., Hansen, M. W., Ozguz, V. H., Esener, S. C. and Marsden, G. C., "Digital free-space optical interconnections: A comparison of transmitter technologies." *Applied Optics* 34(17), pp. 3103–3115, June 1995.
35. Wang, S. C., Dziura, T. G. and Yang, Y. J., "Vertical cavity surface emitting lasers and arrays for optical interconnect and optical computing applications." *Optical Enhancements to Computing Technology* SPIE-1563, pp. 27–33, 1991.
36. Kibar, O., Van Blerkom, D. A., Fan, C., Marchand, P. J. and Esener, S. C., "Small-signal-equivalent circuits for a semiconductor laser." *Applied Optics* 37(26), pp. 6136–6139, September 1998.
37. Martinez, J. A. "Piecewise linear simulation of optoelectronic devices with applications to MEMS." M.S. Thesis, University of Pittsburgh, Department of Electrical Engineering, 2000 (unpublished).
38. Clark, J., Zhou, N., Brown, S. and Pister, K. S. J., "Nodal analysis for MEMS simulation and design," in *Proceedings of Modeling and Simulation of Microsystems Workshop,* Santa Clara, CA, April 1998.
39. Vandemeer, J. E., Kranz, M. S. and Fedder, G. K., "Hierarchical representation and simulation of micromachined inertial sensors," in *Proceedings of Modeling and Simulation of Microsystems Workshop,* Santa Clara, CA, April 1998.
40. Przemieniecki, J. S., *Theory of Matrix Structural Analysis.* McGraw-Hill, New York, 1968.
41. Duncan, W. J., Reciprocation of triply partitioned matrices, Roy, J., *Aeron. Soc.* 60, pp. 131–132, 1956.
42. Rabaey, J. M., *Digital Integrated Circuits, a Design Perspective.* Prentice Hall, Inc., New Jersey, Chapter 11, 1996.
43. ANSYS/Mechanical is registered trademark of ANSYS, Inc.
44. Kurzweg, T. P., Levitan, S. P., Martinez, J. A., Marchand, P. J. and Chiarulli, D. M., "Diffractive optical propagation techniques for a mixed-signal CAD tool." *Optics in Computing (OC2000).* Quebec City, CA, June 2000.
45. Rsoft, Inc.,http://www.rsoftinc.com/

Jose A. Martinez is an electrical engineering Ph.D. student at the University of Pittsburgh. He received his M.S. from the University of Pittsburgh in 2000 in electrical engineering. He received the B.S. in electrical engineering from the Universidad de Oriente (UDO), Venezuela, in 1993. Besides obtaining the magna cum laude laurel in his engineering degree, Mr. Martinez has been granted the Jose Feliz Rivas' medal for high academic achievement by the Venezuelan government (1993), and scholarships by the Venezuelan Fundayacucho Society (1993) and CONICIT-UDO (1994) institution. Since 1997 he has been working in the Optoelectronic Computing Group at the University (PittCAD group). His research interests include analog simulation, reduction order techniques for interconnect analysis, modeling of MEMS and micro-optoelectronic

devices, CAD, VLSI and computer architecture. Mr. Martinez is a member of IEEE/LEOS, and OSA.

Timothy P. Kurzweg is an electrical engineering Ph.D. student at the University of Pittsburgh. He received his M.S. from the University of Pittsburgh in 1997 in electrical engineering. He received his B.S. in electrical engineering from The Pennsylvania State University in 1994. In the summer of 1999, Mr. Kurzweg worked at Microcosm (now Coventor), in Cambridge, MA, and developed an optical methodology to interface within their system-level analysis tool to allow optical MEM simulation. His research interests include modeling and simulation, optical MEMS, CAD, free-space optics, VLSI, and computer architecture. Mr. Kurzweg is a member of IEEE/LEOS, ACM/SIGDA, and OSA.

Steven P. Levitan is the John A. Jurenko professor of electrical engineering at the University of Pittsburgh. He received the B.S. degree from Case Western Reserve University in 1972. From 1972 to 1977 he worked for Xylogic Systems designing hardware for computerized text processing systems. He received his M.S (1979) and Ph.D. (1984), both in computer science, from the University of Massachusetts, Amherst. He is an associate editor for the *ACM Transactions on Design Automation of Electronic Systems*. In 1998 he became Chair of the ACM Special Interest Group on Design Automation and a member of the Design Automation Conference Executive Committee. He is member of OSA, ACM and a senior member of IEEE/CS.

Philippe J. Marchand received his B.S., M.S. and Ph.D. degrees in electrical engineering from the University of Haute Alsace, Mulhouse (France) in 1986, 1987 and 1991 respectively. From 1991 through 1999, he was a research scientist and senior lecturer at the University of California, San Diego with the Optoelectronic Computing Group. His research interests included optical 2-D and 3-D storage, computer generated holography and diffractive optics, optical system design and packaging, optical free-space interconnections, parallel architectures and their applications to parallel optoelectronic computing and telecommunication switching. At UCSD, he worked on developing 3-D packaging technologies for optoelectronic systems and he concurrently worked on the development of models for optoelectronic CAD tools in relation with the University of Pittsburgh. He was a principal investigator for the DARPA funded 3D-OESP Consortium whose goal was to integrated 3D-VLSI and parallel free-space optoelectronic technologies. Since November 1999, he has joined OMM, Inc. as a project director where he is heading the R&D efforts for the development of 3D based MEMS switches. Philippe Marchand has published over 130 articles and papers in refereed journals and scientific meetings, and he holds five patents. He received a Lavoisier fellowship in 1990 from the French Foreign Ministry, the 1991 ADRERUS Thesis prize for his Ph.D. work, and a best paper award at the 1997 Design Automation Conference in Las Vegas. He is a member of IEEE, OSA, and SPIE.

Donald M. Chiarulli is a professor of computer Science at the University of Pittsburgh. He received his M.S. degree in computer science from the Virginia Polytechnic Institute and his Ph.D. also in computer science from Louisiana State University. Dr. Chiarulli's research interests are in photonics and optoelectronic computing systems architecture. Contributions from Dr. Chiarulli's group have included the demonstration of the first all-optical address decoder, several designs for time/space multiplexed data bus architectures, and an all-optical distributed bus arbitration algorithm. Later contributions include the Partitioned Optical Passive Star (POPS) architecture for multiprocessor interconnection networks. This design balanced connectivity and fanout in an optical interconnection network that scaled linearly in optical components over the size of the network. Also proposed with this architecture was a distributed control mechanism that integrated the network control with the control of the memory hierarchy by creating a cache of network paths that could exploit the locality in the network traffic. Other contributions from Dr. Chiarulli's group have included a prediction method for multiprocessor memory access patterns and contributions to the development of a set of tools for optoelectronic CAD. Both of these efforts have earned best paper awards at the International Conference on Neural Networks (ICNN) and the Design Automation Conference (DAC) respectively. Dr. Chiarulli is a member of the IEEE, OSA, and SPIE.